Discovery and Characterization of FMN-Binding β-Glucuronidases in the Human Gut Microbiome

Samuel J. Pellock[1], **William G. Walton**[1], **Samantha M. Ervin**[1],
Dariana Torres-Rivera[1], **Benjamin C. Creekmore**[1], **Grace Bergan**[1],
Zachary D. Dunn[1], **Bo Li**[1], **Ashutosh Tripathy**[2] and **Matthew R. Redinbo**[1,2,3]

1 - *Department of Chemistry,* University of North Carolina at Chapel Hill, Chapel Hill, NC 27599, USA
2 - *Department of Biochemistry and Biophysics,* University of North Carolina at Chapel Hill, Chapel Hill, NC 27599, USA
3 - *Department of Microbiology and Immunology,* and Integrative Program for Biological and Genome Sciences, University of North Carolina at Chapel Hill, Chapel Hill, NC 27599, USA

Correspondence to Matthew R. Redinbo: Department of Chemistry, University of North Carolina at Chapel Hill, Chapel Hill, NC 27599, USA. redinbo@unc.edu
https://doi.org/10.1016/j.jmb.2019.01.013
Edited by Thomas J. Smith

Abstract

The human gut microbiota encodes β-glucuronidases (GUSs) that play key roles in health and disease via the metabolism of glucuronate-containing carbohydrates and drugs. Hundreds of putative bacterial GUS enzymes have been identified by metagenomic analysis of the human gut microbiome, but less than 10% have characterized structures and functions. Here we describe a set of unique gut microbial GUS enzymes that bind flavin mononucleotide (FMN). First, we show using mass spectrometry, isothermal titration calorimetry, and x-ray crystallography that a purified GUS from the gut commensal microbe *Faecalibacterium prausnitzii* binds to FMN on a surface groove located 30 Å away from the active site. Second, utilizing structural and functional data from this FMN-binding GUS, we analyzed the 279 unique GUS sequences from the Human Microbiome Project database and identified 14 putative FMN-binding GUSs. We characterized four of these hits and solved the structure of two, the GUSs from *Ruminococcus gnavus* and *Roseburia hominis*, which confirmed that these are FMN binders. Third, binding and kinetic analysis of the FMN-binding site mutants of these five GUSs show that they utilize a conserved site to bind FMN that is not essential for GUS activity, but can affect K_M. Lastly, a comprehensive structural review of the PDB reveals that the FMN-binding site employed by these enzymes is unlike any structurally characterized FMN binders to date. These findings reveal the first instance of an FMN-binding glycoside hydrolase and suggest a potential link between FMN and carbohydrate metabolism in the human gut microbiota.

Introduction

The human gut microbiome encodes about 5 million genes, outnumbering the human genome by 150-fold [1]. Among the millions of genes in the gut microbiota are those that encode carbohydrate active enzymes (CAZymes), which serve key roles in the metabolism of dietary and endogenous polysaccharides in the human gut [2]. Microbes utilize CAZymes to scavenge sugars from complex carbohydrates in the gut, and the metabolism of these sugars leads to the generation of short-chain fatty acids that have been shown to play key roles in human physiology [3]. Thus, an understanding of the structure and function of these microbial enzymes is essential for elucidating their roles in human health and disease.

One group of gut bacterial CAZymes are β-glucuronidases (GUSs). Microbial GUS enzymes are unique among CAZymes because they play roles in the metabolism of both polysaccharides and drug metabolites. For example, GUSs are capable of catalyzing the hydrolysis of glucuronate-containing polysaccharides, such as heparin and hyaluronate, as well as small-molecule drug glucuronides like SN-38-G, the inactive metabolite of the anticancer drug irinotecan, and NSAID glucuronides [4–7]. Drug glucuronides are generated in the liver by uridine diphosphate glucuronosyl transferases and then secreted into the GI tract

where they are processed by bacterial GUSs, which reverse the actions carried out by the host (Fig. S1) [8]. Many other glucuronides, primarily glucuronate-containing polysaccharides, are present in the gut, including glycosaminoglycans, such as heparin and hyaluronate, as well dietary, bacterial, and plant polysaccharides like pectin, sphingans, and xylans [9]. Given the importance of these diverse molecules in therapeutics, nutrition, and homeostasis of the gut microbiota, it is critical to understand the structure and function of the microbial enzymes that process them.

Utilizing metagenomic data and structural analyses, we recently cataloged 279 unique GUS enzymes from the Human Microbiome Project (HMP) stool sample database [4]. Only a few bacterial GUSs from the human gut have a characterized structure and function, and most of these characterized GUSs do not have a clear function in the gut microbiota. Here we characterize the GUS from *Faecalibacterium prausnitzii* L2–6 and show that it binds flavin mononucleotide (FMN) at a distant surface site. While glycoside hydrolases are among the most well-characterized enzymes in biochemistry, this is the first observation of a flavin-bound glycoside hydrolase. Utilizing these structural and functional data, we screened GUSs found in the HMP stool sample database for key FMN-binding residues and identified 14 additional FMN-binding GUSs. We characterized four of these biochemically and determined the crystal structures of two, which confirm a structurally conserved FMN-binding site. We further show by a comprehensive review of the PDB that the GUSs characterized here bind FMN in a manner unlike any previously characterized FMN-binding proteins. These data reveal the first association between FMN and a glycoside hydrolase, suggesting a link between FMN and carbohydrate metabolism in the human gut microbiota.

Results

Discovery of an FMN-binding GUS from the human gut microbe *F. prausnitzii* L2–6

Utilizing structural, functional, and sequence data on characterized bacterial GUS enzymes [10–12], metagenomic analysis of the HMP stool sample database revealed 279 unique GUS enzymes in the human gut microbiome [4]. Most of these proteins remain uncharacterized; thus, we initiated an effort to express and examine representative GUSs from the distinct classes discovered. Surprisingly, the gene synthesis, protein expression, and purification of a GUS from the human gut bacterium *F. prausnitzii* L2–6 (*Fp2*GUS) yielded a yellow protein product (Fig. 1a). Absorbance scan of purified *Fp2*GUS displayed a profile characteristic of a flavin-binding protein (Fig. 1a), and LC–MS analysis of purified *Fp2*GUS revealed the mass for FMN (Fig. 1b).

While FMN is bound upon expression and purification of *Fp2*GUS, absorbance scans revealed that the stoichiometry of binding was approximately 0.42:1 (FMN:*Fp2*GUS), suggesting that vacant FMN-binding sites may be present (Fig. S2). Thus, we utilized isothermal titration calorimetry (ITC) to measure the binding affinity of *Fp2*GUS for FMN using this partially occupied sample, which revealed a K_d of 1.05 μM (Fig. 1c). Together, these data establish that *Fp2*GUS is an FMN-binding glycoside hydrolase.

Crystal structure of *Fp2*GUS reveals an FMN-binding site

To further understand the FMN-binding nature of *Fp2*GUS, we determined its crystal structure to 2.55-Å resolution (Table S1). The *Fp2*GUS crystal structure revealed an FMN-binding site approximately 30 Å away from the active site, formed by two alpha helices from the core TIM barrel fold (cyan) and two jellyroll-like β-sandwich domains (blue and green) (Fig. 2a). The FMN-binding site is primarily formed by Y154 and F179, which make π–π stacking interactions with the isoalloxazine ring of FMN (Fig. 2b, c). In addition to these two aromatic residues, K356 forms an ionic interaction with the phosphate of FMN, D151 forms a hydrogen bond with the amide nitrogen of the isoalloxazine ring, M161 participates in hydrophobic interactions with the isoalloxazine ring, and Y363 makes an edge-to-face π interaction with the isoalloxazine ring (Fig. 2b, c). Computational generation (DFT theory: wB97x-D 6-31G*) of the electrostatic potential map of FMN reveals that the most electron poor region of the isoalloxazine ring makes π–π stacking interactions with the negative faces of Y154 and F179 (Fig. 2c). In addition to the unprecedented FMN-binding site, *Fp2*GUS is also a trimer as identified from the crystal structure and size exclusion chromatography with multi-angle light scattering (Fig. S2D, E). Together, these structural data reveal that *Fp2*GUS binds to FMN via numerous π–π interactions at a site located 30 Å from the active site.

FMN-binding site of *Fp2*GUS integral to protein stability

To determine the role of the FMN-binding site in the structure and function of *Fp2*GUS, we performed site-directed mutagenesis of the following residues that contact FMN in the crystal structure: D151, Y154, F179, K356, and Y363 (Fig. 2b, c). Size exclusion chromatography and SDS-PAGE analysis revealed that each *Fp2*GUS mutant yielded unstable protein products, with a smaller amount of full-length and soluble protein relative to wild-type (WT), suggesting that the FMN-binding site helps stabilize *Fp2*GUS (Fig. S3A, B). Absorbance scans of the intact peaks of the *Fp2*GUS mutants revealed either reduced or no flavin-binding profiles, suggesting reduced FMN binding (Fig. S3C).
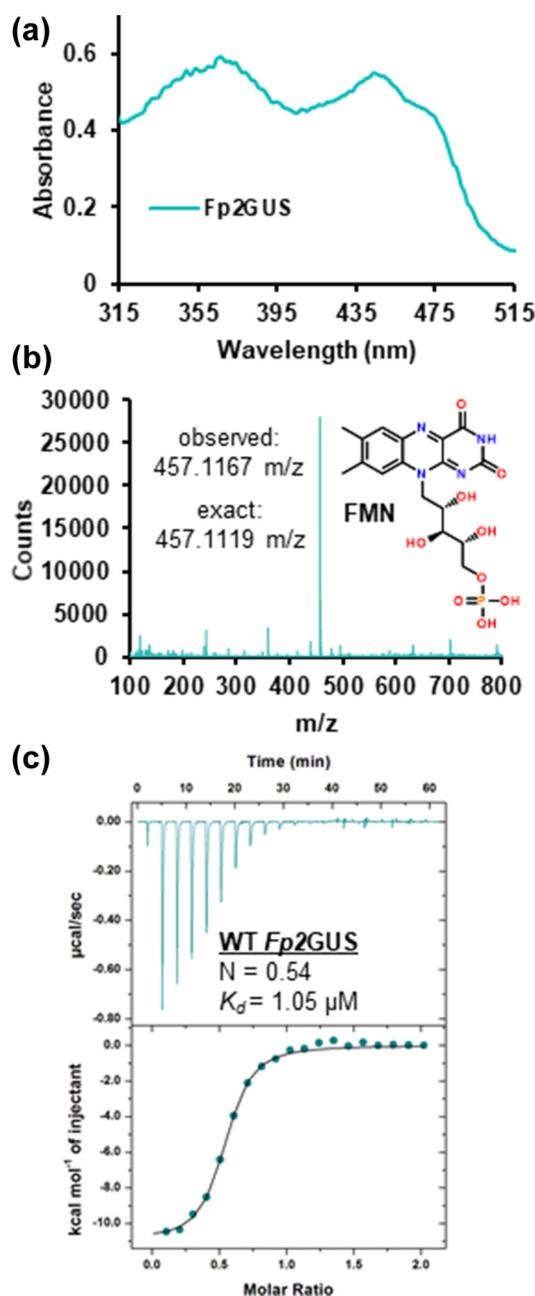
(a)

(b)

(c)

Fig. 1. Discovery of an FMN-binding GUS from the human gut microbe *F. prausnitzii* L2–6. (a) Absorbance scan of purified *Fp2*GUS in yellow, reveals a UV profile characteristic of a flavin-binding protein. (b) Mass spectrum of purified *Fp2*GUS contains mass for FMN (observed mass: 457.1167 *m/z*, exact mass: 457.1119 *m/z*). (c) Titration of WT *Fp2*GUS with FMN monitored by ITC reveals binding constant of 1.05 and an FMN occupancy for WT *Fp2*GUS of 46% (N = 0.54).

The K356A, D151A, and Y363A mutants of *Fp2*GUS still bind FMN with similar potency to the WT enzyme, suggesting that while these residues appear to form

key contacts with FMN in the crystal structure, their overall contribution to binding FMN is negligible (Fig. S3D). Thus, it would appear that, for the K356A, D151A, and Y363A mutant forms of *Fp2*GUS, less of the protein was bound to FMN, but for the fraction that did bind the cofactor, binding affinity remained similar to WT. In contrast, Y154A and F179A displayed significantly reduced binding to FMN, along with reduced stability (Fig. S3D). Finally, interestingly, while stability is lost upon mutation of the FMN-binding site, the catalytic activities of the *Fp2*GUS mutants are not significantly different from the WT protein (Fig. S3E). Together, these data suggest that the FMN-binding site of *Fp2*GUS plays a key role in the stability of the protein but does not affect catalysis.

Bioinformatic analysis identifies 14 additional FMN-binding GUSs in the human gut

Using the structural and mutagenesis data from the *Fp2*GUS FMN-binding site as a guide, we analyzed GUS sequences from the HMP stool sample database to determine if other GUSs may be FMN binders. Out of the 278 proteins examined, a total of 14 sequences, in addition to *Fp2*GUS, contained the key FMN-binding residues (Figs. 3a and S4). Generation and analysis of a sequence similarity network of GUS enzymes from the HMP stool sample database revealed that the one confirmed and 14 putative FMN-binding GUSs cluster into three clades, all of which contain GUSs exclusively from the previously defined No Loop (NL) structural category, which refers to the absence of an active site adjacent loop shown to play key roles in substrate specificity (Fig. 3a) [4]. BLAST and SignalP 4.1 analysis of the putative FMN-binding GUS sequences reveal that they all come from bacteria in the class Clostridiales and do not contain signal peptide sequences, suggesting that they are intracellular [13,14]. Further bioinformatic analysis utilizing the Enzyme Function Initiative Genome Neighborhood Tool (EFI-GNT) revealed two distinct genetic neighborhoods surrounding the FMN-binding GUS genes (Fig. 3b) [15]. Four of the 15 putative FMN binders, including *Butyrivibrio fibrisolvens*, two strains of *Roseburia inulinivorans*, and *Roseburia hominis* are flanked by genes encoding a β-glucosidase (GH1), an α-L-rhamnosidase (GH78), and a xylose isomerase (ISO) (Fig. 3b). The remaining 11 FMN-binding GUS genes are flanked by AraC transcriptional regulators and MFS transporters, proteins that likely sense and transport glucuronate-containing molecules (Fig. 3b). Taken together, a family of FMN-binding GUS enzymes appears to be encoded by the human gut microbiome.

Biochemical characterization confirms FMN binding of bioinformatic hits

From the 14 additional putative FMN-binding GUS sequences identified, we selected the following four GUS genes to synthesize, express, and purify:
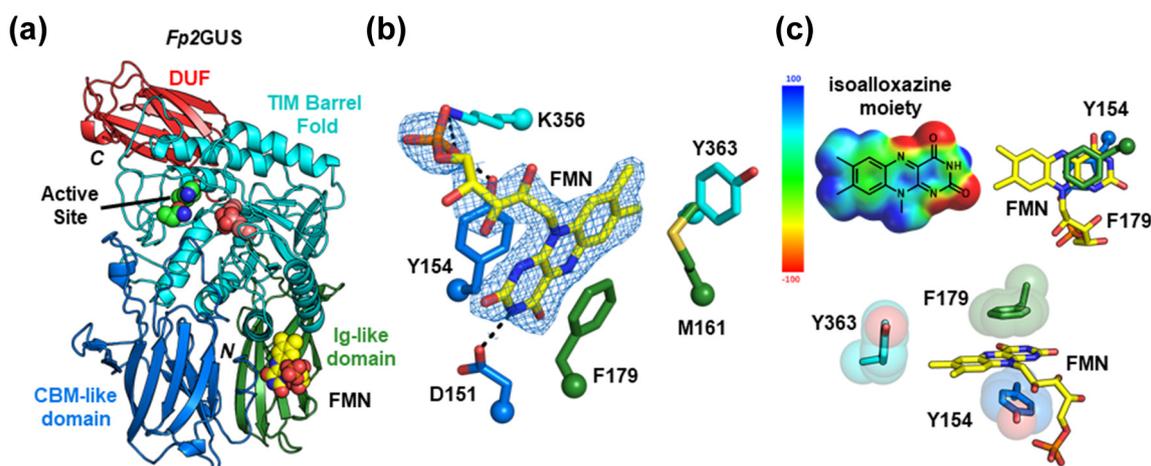
Fig. 2. Crystal structure of *Fp2*GUS reveals an FMN-binding site. (a) Monomer of *Fp2*GUS with active site glutamates shown as deep salmon spheres, NxK motif shown as green spheres, and FMN shown as yellow spheres. (b) FMN-binding site of *Fp2*GUS with 2Fo-Fc density shown at 1.0 σ. (c) Electrostatic potential map (DFT theory: wB97x-D 6-31G*) of FMN highlights an array of π interactions between FMN and *Fp2*GUS, including π–π stacking between the electron poor region of the isoalloxazine moiety and the electronegative faces of Y154 and F179 (right and bottom), as well as an edge-to-face interaction with Y363.

R. inulinivorans (*Ri*GUS), *R. hominis* (*Rh2*GUS), *B. fibrisolvens* (*Bv*GUS), and *Ruminococcus gnavus* (*Rg3*GUS). These four enzymes share between 40% and 46% sequence identity with *Fp2*GUS (Fig. S5D). Upon expression and purification, all four of the selected sequences yielded yellow protein products with a flavin-binding absorbance profile (Fig. 3c), displayed the mass for FMN by LC–MS (Fig. 3d), and bound FMN with dissociation constants that range from 60 nM (*Rg3*GUS) to 1.27 µM (*Bv*GUS) (Fig. 4a and Table S2). These results validate our structure-guided bioinformatic identification of FMN-binding GUSs from the gut microbiome.

To confirm that the FMN-binding sites of *Rh2*GUS, *Rg3*GUS, *Bv*GUS, and *Ri*GUS were similar in molecular nature to that identified in *Fp2*GUS, we mutated the residue corresponding to Y154 in *Fp2*GUS in each protein to alanine (Figs. 2b and 4b). Each of these mutants was no longer yellow or displayed significantly reduced yellow color, and no longer displayed a flavin-binding profile (Fig. S5C). Interestingly, unlike the FMN-binding site mutants of *Fp2*GUS, these mutants yielded stable protein products (Fig. S5A, B). The mutant GUSs Y152A *Ri*GUS, Y159A *Rg3*GUS, and Y159A *Rh2*GUS were still capable of binding FMN, although they did so with much weaker affinities (Fig. 4a and Table S2). Together, these data demonstrate that FMN-binding GUSs utilize a conserved motif to bind FMN, and that mutation of FMN-binding residues has differential effects on distinct GUS enzymes.

Structural analysis of *Rh2*GUS and *Rg3*GUS reveals a conserved FMN-binding site

We next determined the crystal structures of *Rh2*GUS and *Rg3*GUS to 2.4 and 2.8 Å resolution,

respectively. *Rh2*GUS and *Rg3*GUS share high structural similarity to *Fp2*GUS, aligning with RMSD values of 1.6 and 1.8 Å over 624 Cα positions, respectively (Fig. S6A). Similar to *Fp2*GUS, *Rh2*GUS and *Rg3*GUS both contain an FMN-binding site that is approximately 30 Å from the active site (Figs. 4b and S6B). The FMN-binding site of *Rh2*GUS and *Rg3*GUS is similar to *Fp2*GUS, except that a lysine replaces the methionine interacting with the isoalloxazine ring (Fig. 4b). While the quaternary structure of *Rg3*GUS is unclear based on the crystal structure (Fig. S6C), it appears that *Rh2*GUS may form either a unique dimer or tetramer based on its crystal structure (Fig. S6D). SEC-MALS analysis supports this conclusion, with predicted dimer–tetramer mixtures for both *Rh2*GUS and *Rg3*GUS (Fig. S7). Therefore, we conclude that FMN-binding GUSs in the gut microbiota contain similar FMN-binding sites and similar tertiary structures, but have distinct quaternary structures.

The FMN-binding site is not required for GUS activity

To assess the role of the FMN-binding site in the catalytic function of these GUSs, we determined the catalytic properties of the WT and FMN-binding site mutants. Each GUS was able to hydrolyze the fluorescent reporter substrate 4-methylumbelliferyl glucuronide (4-MUG) (Table S3). The WT and FMN-binding mutants displayed nearly identical k_{cat} values (Fig. 5a), but the FMN-binding mutants generally displayed higher K_M values (Fig. 5b). For example, the FMN-binding mutants of *Rh2*GUS, *Rg3*GUS, and *Bv*GUS all display significantly higher K_M values than WT (Fig. 5b and Table S3). In contrast, the K_M values of the FMN-binding mutants
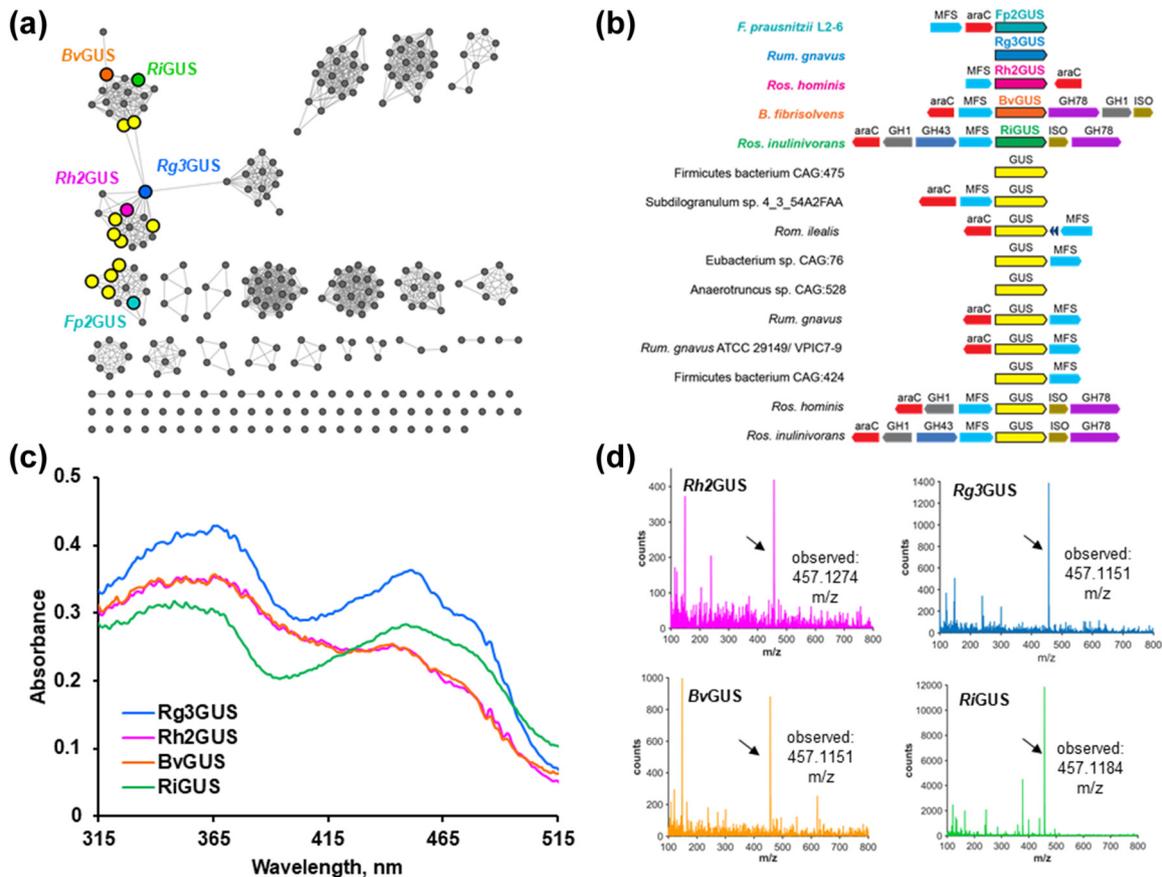
Fig. 3. Bioinformatic analysis predicts 14 additional FMN-binding GUS enzymes from the human gut microbiota. (a) SSN of the HMP GUSome with putative FMN binders as larger, outlined circles, and those that were synthesized and characterized further are labeled. Alignment score value utilized to generate this SSN is 10^{-220}, and sequences were acquired from the HMP stool sample database. (b) Genome neighborhood diagrams of putative FMN-binding GUSs. (c) Absorbance scans of purified *Rh2*GUS, *Rg3*GUS, *Bv*GUS, and *Ri*GUS reveal flavin binding profile. (d) Mass spectra of purified *Rh2*GUS, *Rg3*GUS, *Bv*GUS, and *Ri*GUS reveal mass for FMN.

of *Fp2*GUS and *Ri*GUS were not significantly different from the WT enzymes. Thus, these data confirm that the FMN-binding site is not necessary for catalytic function but does increase the K_M for some of these FMN-binding GUSs.

The GUS FMN-binding site is unique among characterized FMN-binding proteins

Because the FMN-binding site does not affect catalysis, we performed a comprehensive search of the PDB in an attempt to deduce a function for this site by looking for similar structures. We examined the PDB for FMN-bound structures, which identified 1056 deposited structures, with 438 non-redundant entries. We then visually inspected these 438 non-redundant structures in PyMOL to determine if any other FMN-binding proteins bind flavin in the same manner as the GUSs characterized in this work. In agreement with previous analyses, the most common fold we en-

countered was the TIM-barrel fold, and we use Old Yellow Enzyme (PDB: 1OYB) as an example of how FMN binds at the β-barrel core of the fold (Fig. 6). Interestingly, while the FMN-binding GUS enzymes characterized here are also TIM-barrel-containing proteins, they bind FMN on the exterior of this fold, not the interior, and two adjacent β-sandwich domains contribute to the FMN-binding site as well (Figs. 2a and 6). The second most common FMN-binding fold is the flavodoxin fold, named after the protein flavodoxin (PDB: 1FLD), which binds FMN at the edge of a β-sheet flanked on both sides by α-helices (Fig. 6). In addition to the TIM-barrel fold and flavodoxin fold, we identified 18 other structurally distinct FMN binders out of the 438 non-redundant structures (Fig. S8). These other folds sample a wide variety of structural motifs to bind FMN, but none bind FMN outside the TIM barrel core as observed for the GUS enzymes characterized here (Fig. S8). Thus, the FMN-binding site in gut microbial GUS enzymes is unique.
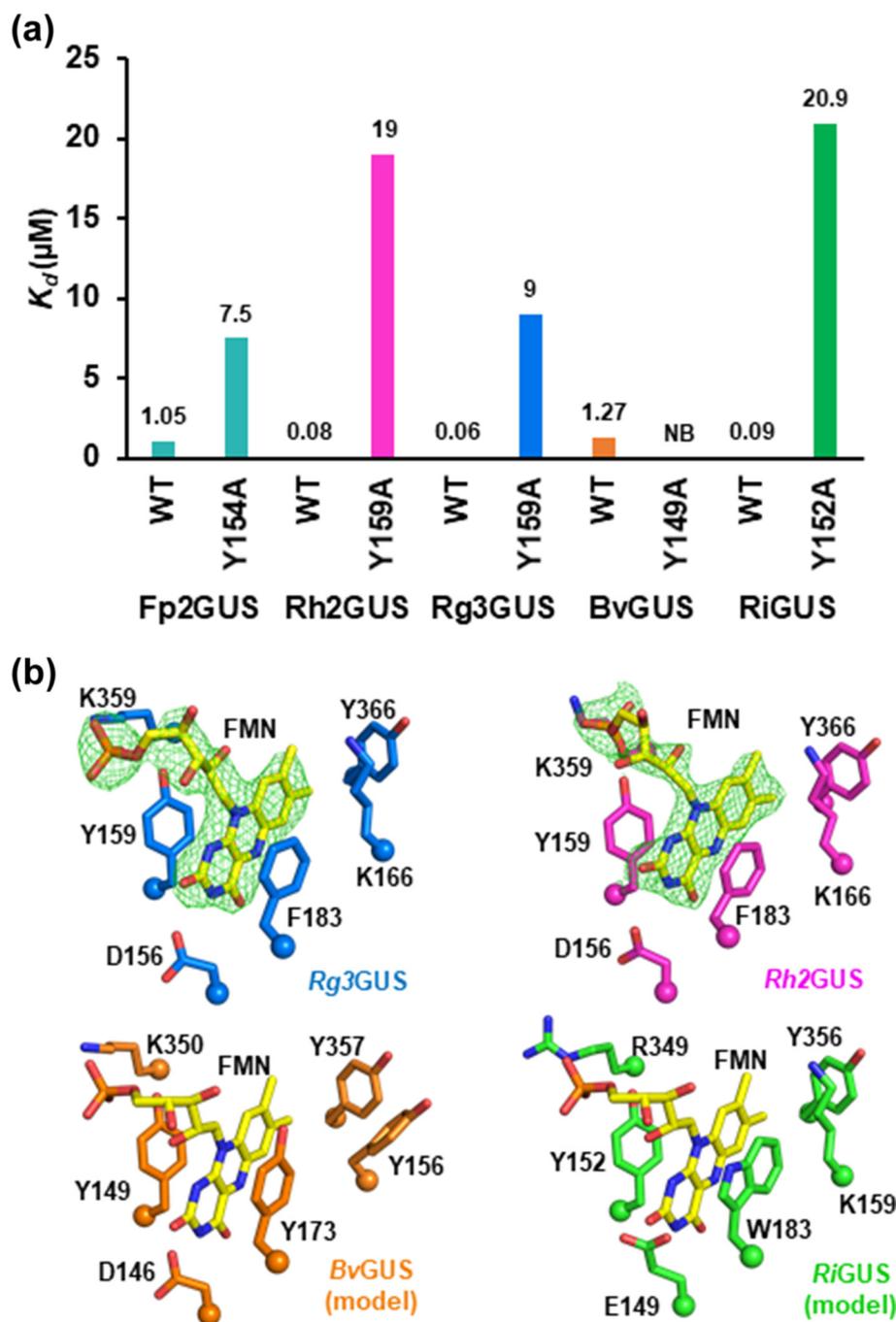
Fig. 4. Binding studies and structural analysis demonstrate that GUS enzymes utilize a conserved motif to bind FMN. (a) Binding affinities (K_d) of GUS enzymes and FMN-binding site mutants for FMN as determined by ITC. (b) Structures of FMN-binding sites as determined by crystallography for *Rg3*GUS (blue) and *Rh2*GUS (magenta) and by template-guided modeling for *Bv*GUS (orange) and *Ri*GUS (green). 2Fo-Fc density for FMN shown at 1 σ.

As an additional, distinct screen to confirm the novelty of this FMN-binding site, we performed a PDBeFold search to find similar structures to the GUS enzymes characterized here. The top hits were all previously characterized GUS enzymes, with the most similar being *Bf*GUS (PDB: 3CMG) and *Bu*GUS-3 (PDB: 6D1P). Inspection of these structures revealed the common GH2 GUS fold, but the absence of the key FMN-binding residues identified in the GUSs characterized here (Fig. S9B). Taken together, this structural
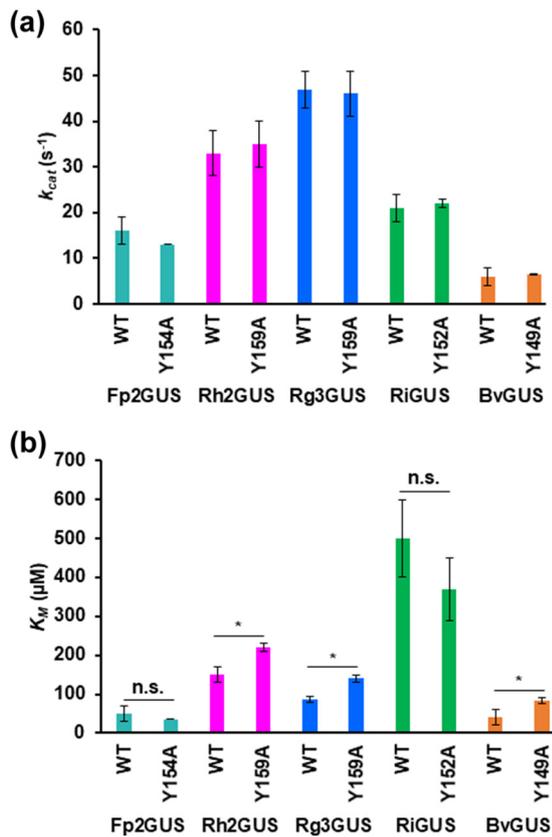
Fig. 5. Kinetic studies of FMN-binding GUSs show that FMN-binding site is not required for GUS activity. (a) Catalytic turnovers (k_{cat}) of FMN-binding GUSs and their respective FMN-binding site mutants. (b) Michaelis constants (K_M) of FMN-binding GUSs and their respective FMN-binding site mutants. * represents p-value < 0.05.

analysis demonstrates that the GUSs characterized here are unique among FMN-binding proteins characterized to date.

Discussion

Here we structurally and functionally characterize a family of FMN-binding GUS enzymes. Characterization of the GUS from the human gut bacterium *F. prausnitzii* L2–6 revealed a novel FMN-binding glycoside hydrolase and its crystal structure guided the search for other FMN-binding GUS enzymes in the HMP stool sample database. We identified 14 more unique FMN binders, 4 of which were characterized and confirmed to bind FMN. Our characterization of the WT and FMN-binding site mutants of these GUSs suggests that FMN plays a key role in the stability of *Fp2*GUS, but not for the other FMN binders (Figs. S3A, B, and S5A, B). Furthermore, we show that mutating the FMN-binding site does not significantly affect enzyme activity, suggesting that the FMN-binding site is not essential for GUS function

(Fig. 5). Together, these data reveal the first FMN-binding glycoside hydrolase, show that there is a family of FMN-binding glycoside hydrolases in the gut microbiota, the FMN-binding site is not required for the function of the enzyme, and reveal a novel FMN-binding site among FMN-binding proteins structurally characterized to date.

While previously characterized bacterial GUSs share similar tertiary structures to the FMN-binding GUSs discovered here, none contain the residues necessary to form the FMN-binding site (Fig. S9B). *Fp2*GUS shares RMSDs of 3.4 Å (across 528 Cα positions), 2.1 Å (624 Cα), and 2.7 Å (632 Cα) with *Escherichia coli* GUS (*Ec*GUS, PDB: 3LPF), *Bacteroides fragilis* GUS (*Bf*GUS, PDB: 3CMG), and *Bacteroides uniformis* GUS 2 (*Bu*GUS-2, PDB:5UJ6), respectively. The C-terminal domain of *Fp2*GUS, *Rh2*GUS, and *Rg3*GUS was disordered in the crystal structures elucidated here, with approximately 100 residues missing from each individual chain. This unresolved region may form a carbohydrate binding module, a structural feature seen at the C-terminus of two GUSs previously characterized from *B. uniformis* [4,5]. The active site of the FMN-binding GUSs characterized here is similar to previously characterized GUS enzymes, containing both the two conserved catalytic glutamates and the NxK motif (Fig. S9C) [4].

The FMN-binding GUSs characterized here add to the diverse quaternary structures discovered recently among gut bacterial GUSs. Five distinct oligomerization states have been previously observed, including three distinct tetramers and two unique dimers (Fig. S10). Here we uncover two additional tetrameric states, a trimer (*Fp2*GUS) and an apparent dimer–tetramer mix (*Rh2*GUS) (Figs. S2D and S6D). The oligomeric states of bacterial GUSs have previously been shown to play key roles in GUS function. For example, the tetrameric loop 1 (L1) GUS enzymes (*E. coli* GUS, PDB: 3LPF, Fig. S9A) have small hydrophobic pockets around their active sites due to overlapping loops of adjacent protomers, limiting their substrate scope to lipophilic, small-molecule glucuronides [4]. Most other bacterial GUSs have open, solvent-exposed active sites, allowing access to large, polar substrates like glucuronate-containing polysaccharides [4,5]. Both the trimer of *Fp2*GUS and the dimer–tetramer mix of *Rh2*GUS fit within this latter group of GUSs with solvent exposed active sites, suggesting that their preferred substrates are likely glucuronate-containing polysaccharides.

The cognate substrates of some of these FMN-binding GUSs may be extracellular polysaccharides. The EFI-GNT analysis of the GUS genes from *B. fibrisolvens*, two strains of *R. inulinivorans*, and *R. hominis* revealed nearby CAZymes, including a β-glucosidase (GH1), an α-L-rhamnosidase (GH78), and a xylose isomerase (ISO) (Fig. 3b). Together, these genes may coordinate the degradation of an extracellular polysaccharide within the group known as
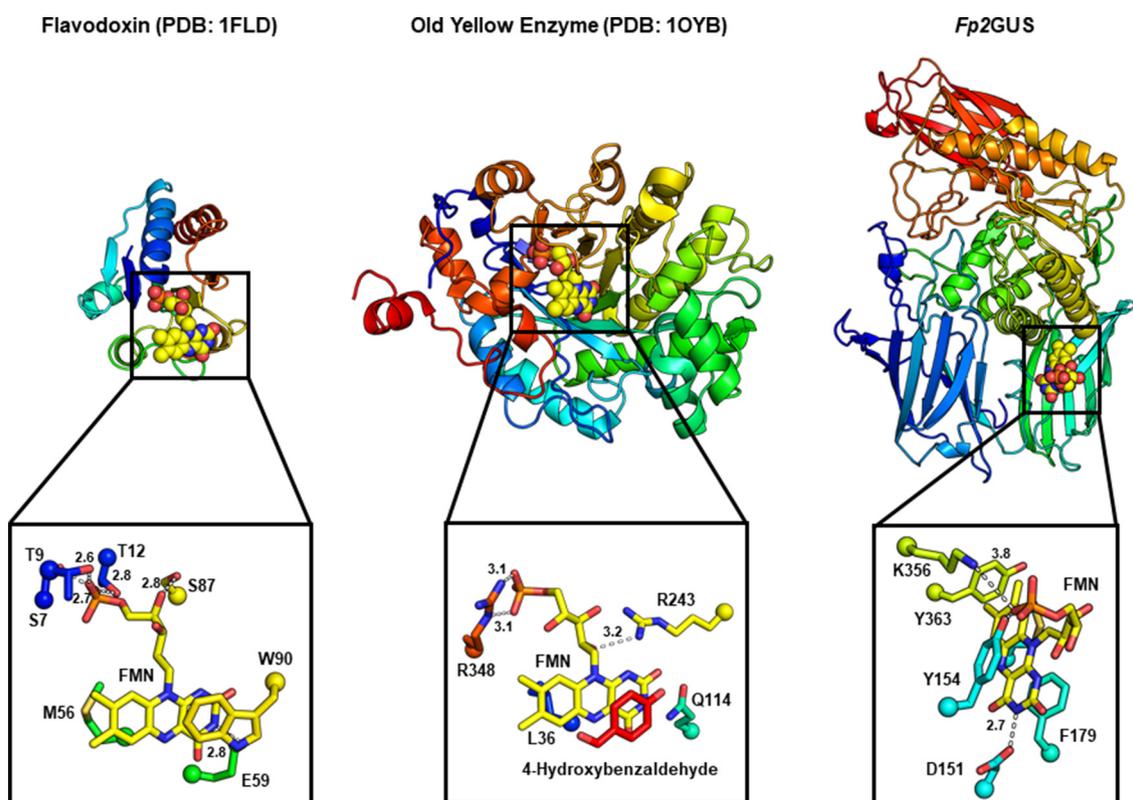
Fig. 6. Structural comparison of FMN-binding proteins reveals that FMN-binding GUSs identified here bind FMN in a unique manner. (A) Structure of flavodoxin (PDB: 1FLD). (B) Old Yellow Enzyme (PDB: 1OYB), and (C) *Fp2*GUS with zoom-in of their respective FMN-binding sites.

sphingans. The repeating unit of sphingans contains α-linked rhamnose, β-linked glucose, and β-linked glucuronate moieties, all of which could be processed by the genes present in these genetic loci (Fig. S11) [16]. Indeed, previous studies have associated orthologs of these enzymes with the catabolism of sphingans and related exopolysaccharides [17,18]. Detailed future studies with relevant polysaccharide substrates will be required to identify the cognate substrates of these FMN-binding GUSs.

The discovery of FMN-binding GUSs suggests a link between polysaccharide metabolism and FMN in the human gut. Interestingly, the pentose and glucuronate interconversion pathway contains a biosynthetic route that shunts glucuronate into the riboflavin metabolism pathway, responsible for the generation of FMN and FAD in bacteria (Fig. S12). A myriad of enzymes is needed to transform glucuronate to D-ribulose-5-phosphate, which can generate FMN in combination with GTP (Fig. S12). If glucuronate released by the FMN-binding GUSs is converted into FMN, it could serve as a positive feedback loop for GUS activity. However, this seems unlikely as we observed that FMN has only a small impact on the activity of these enzymes.

We note in our three structures of FMN-binding gut microbial GUS enzymes that a channel exists on the surface of each protein that provides access to N5 of the bound flavin, which is a key site for redox chemistry (Fig. S13). It is possible that a small molecule could access this site to utilize FMN for oxidation–reduction reactions. While this is speculative, two features of the FMN-bound GUS enzymes make this potentially accurate. First, the non-FMN-binding GUS proteins have residues that block this channel, while the channel remains open in the FMN-bound GUS enzymes. Second, while many GUS enzymes have signal sequences and may be exported to the periplasm, all the FMN-binding GUS enzymes detected to date lack a signal sequence and thus are expected to remain intracellularly localized, a place where redox chemistry can be better controlled and utilized by the cell. Future work will be required to determine whether this channel provides functionally relevant access to the bound FMN of these particular GUS enzymes.

Structural and functional analysis reported here leaves the role of FMN in GUS function unclear. While FMN was a key factor for stability in *Fp2*GUS, it did not have a major effect on the activity or stability of the other four FMN-binding GUSs characterized.

Based on structural comparison with previously characterized FMN-binding proteins, it also does not appear to be similar to any oxidoreductases or electron transport-like proteins characterized to date. Future studies will be necessary to unravel the role this cofactor plays in GUS function, whether it is present for stability like that observed for *Fp2*GUS, or impacts catalytic efficiency like that observed for some of the other FMN-binding GUSs characterized. Another possibility is that FMN may perform a completely different function from GUS activity. For example, these enzymes may have binding partners that can utilize FMN in ways that are not clear from studying these GUSs in an isolated system.

Conclusion

Here we characterize a unique set of FMN-binding GUS enzymes from the human gut microbiome. We determined the crystal structure of a GUS from *F. prausnitzii* and show that it binds FMN at a surface site approximately 30 Å from the active site. Using these structural data, we screened the HMP stool sample metagenomic database and identified 14 additional putative FMN binders. We characterized four of these putative FMN-binding GUS enzymes *in vitro* and confirmed that they are *bona fide* FMN binders, with binding affinities as low as 60 nM. Site-directed mutagenesis of all five FMN binders and crystals structures of the FMN-binding GUS from *R. hominis* and *R. gnavus* reveal a conserved FMN-binding site. Kinetic studies of the FMN-binding mutants suggest that the FMN-binding site is not necessary for GUS function, but mutations to this site can impact the K_M. Lastly, a structural bioinformatic search demonstrates that no other characterized FMN binders interact with FMN like that observed with these FMN-binding glycoside hydrolases.

Methods

Gene synthesis, expression, and purification of FMN-binding GUSs

Genes for *Fp2*GUS, *Rh2*GUS, *Rg3*GUS, *Bv*GUS, and *Ri*GUS were synthesized by BioBasic and incorporated into a pLIC-His vector via ligation independent cloning, and resultant plasmids were transformed into BL21-G *E. coli* cells. Glycerol stocks were made from overnights and snap frozen and stored at −80 °C. Verification of successful transformation and sample integrity were determined by DNA sequencing.

Cultures of 100 mL LB with ampicillin were inoculated with glycerol stock and incubated overnight at 37 °C with shaking at 225 rpm. For protein expression, 50 mL of the overnight, approximately 40 µL Antifoam 204,

and 750 µL of 2000x ampicillin were added to 1.5 L LB in a 2.5-L Erlenmeyer flask and incubated at 37 °C at 225 rpm. At an OD was approximately 0.6, the temperature was reduced to 18 °C and induced with IPTG (100 mM) at an OD of approximately 0.8 and incubated overnight with shaking at 225 rpm. Cultures were spun down in a Sorvall Instruments RC-3B centrifuge at 4500*g* for 25 min in 1 L round, flat bottom plastic bottles. Cultures were resuspended in LB and transferred to a 50-mL falcon tube and spun down in a ThermoScientific Sorvall ST 40R centrifuge for 15 min at 5000*g*. Supernatant was discarded and proteins were stored at −80 °C until purification.

Cell pellets were lysed in 30 mL Nickel A buffer [20 mM KH_2PO_4, 500 mM NaCl, 50 mM imidazole (pH 7.4)] with DNase, lysozyme, and a Roche EDTA-free protease inhibitor tablet. The resultant cell slurry was sonicated on a Fischer Scientific Sonic dismembrator model 500 twice with 1 s pulses for 1.5 min. The resultant lysate was subsequently spun down on a Beckman Coulter J2-HC centrifuge for 1 h at 17,000 rpm. The supernatant was subject to filtration with a 0.22-µm filter prior to purification.

Protein was first purified with an Aktaxpress FPLC (Amersham Bioscience) via a Ni NTA column. Protein was eluted in one step using Nickel B buffer [20 mM KH_2PO_4, 500 mM NaCl, 500 mM imidazole (pH 7.4)]. Fractions were collected and concentrated with a 50 K centrifilter at 3000*g* for 15 min if necessary before size exclusion chromatography. The eluent was then subject to size exclusion chromatography on a HiLoadTM 16/60 Superdex 200 gel filtration column. Size exclusion buffer was utilized for elution [20 mM Hepes, 50 mM NaCl (pH 7.4)]. Fractions were collected and an SDS-PAGE gel was performed to assess purity and stability of the enzyme. Protein concentration was determined on an ND-1000 spectrophotometer and then snap frozen in liquid nitrogen and stored at −80 °C.

Side-directed mutagenesis of FMN-binding GUSs

All mutants were created via site-directed mutagenesis. Mutagenesis primers were synthesized by Integrated DNA technologies. Mutant plasmids were sequenced by Eton Bioscience to confirm successful mutagenesis.

Absorbance scans of WT and mutant GUSs and stoichiometry determination

Absorbance scans of WT and mutant GUSs were determined in a BMG labtech PHERAstar plate reader. All proteins were analyzed at 50 µM in 96-well Costar half area, clear, flat bottom UV-transparent plates. Resultant absorbance profiles were plotted in Microsoft Excel 2013.

Liquid chromatography–mass spectrometry

Protein samples were diluted in sizing buffer to approximately 10 µM and applied to a 0.22-µm filter prior to analysis. Separation was carried out on a Viva C4 5-µm 150 × 2.1-mm column. Solvent A was 0.1% formic acid in water, and solvent B was 0.1% formic acid in acetonitrile. FMN-binding proteins were eluted using a linear gradient of 5% solvent B to 60% B for 20 min, held for 1 minute, and then an additional linear gradient from 60% to 95% B for 17 min. Samples were analyzed using an Agilent Technologies 6520 Accurate-Mass Q-TOF LC–MS instrument in positive-ion mode, and the resultant data were analyzed in MassHunter Qualitative Analysis B0.06.00 software.

ITC to determine FMN-binding affinity

ITC experiments were performed on a MicroCal AutoITC-200. All experiments were performed at 25 °C with 120-s intervals, reference heat of 7 kcals/s, and 20 injections total. Protein and ligand were prepared in size exclusion buffer, and all ITC data were corrected with a control experiment of ligand dilution into buffer. Protein and ligand concentrations were varied depending on the amount of FMN present as determined from absorbance scans.

Crystal formation, preparation, and data collection of FMN-binding GUSs

*Fp2*GUS was crystallized via the sitting drop method in Hampton Research 3-well Crystallization Plates (Swissci) at 11.1 mg/mL in 0.2 M magnesium chloride, 10% w/v PEG 3000, and 0.1 M sodium cacodylate. Incubation at 20 °C resulted in crystal formation after 11 days. *Rg3*GUS was crystallized by the hanging drop vapor diffusion method at 20.4 mg/mL in 0.13 M magnesium acetate and 10% PEG 8000. Incubation at room temperature yielded crystals of *Rg3*GUS after 2–3 days. *Rh2*GUS was crystallized by the hanging drop vapor diffusion method at 14.9 mg/mL in 0.2 M calcium acetate and 50% PEG 8000 at room temperature after approximately 30 days. All crystals were looped and cryoprotected in their crystallant plus 20% glycerol before storing in liquid nitrogen.

X-ray diffraction experiments were performed at GM/CA ID-D and ID-B beam sources. Standard collection methods were followed, and resultant data were reduced in XDS and scaled in aimless. The structure of *Fp2*GUS was solved via molecular replacement in Phenix using the single-component MR-Phaser program with *B. fragilis* GUS (3CMG) as the search model. *Rg3*GUS and *Rh2*GUS were solved by molecular replacement using the *Fp2*GUS structure as the search model. Final coordinates were deposited in the RCSB PDB with PDB codes 6MVF, 6MVG, and 6MVH for *Fp2*GUS, *Rg3*GUS, and *Rh2*GUS, respectively.

Bioinformatic analysis of HMP stool sample database for identification of FMN-binding GUSs

We utilized the previously generated database of GUS sequences from the HMP stool sample database to screen for putative FMN-binding GUSs [4]. To identify other FMN-binding GUSs, we first performed pairwise sequence alignments of each GUS sequence against *Fp2*GUS and rejected those with less than 25% sequence identity. The remaining sequences were screened with a length requirement of 700–800 residues and contained the FMN-binding site residues (or similar residues) identified in *Fp2*GUS: D, E, or other small residue at position 151; Y, F, or W at position 154; F, Y, or W at position 179; K or R at position 356; and Y, F, or W at position 363 (Fig. S3).

In vitro kinetic assay for k_{cat} and K_M determination of FMN-binding GUSs

To assess the activities of WT and mutant GUSs, we measured their ability to hydrolyze the fluorescent reporter substrate 4-MUG. Reactions were performed in black Costar 96-well plates with a flat, clear bottom, and reaction volumes were as follows: 5 µL water, 5 µL buffer [25 mM Hepes, 25 mM NaCl (pH 6.5), or 25 mM $NaCH_3CO_2^-$ and 25 mM NaCl (pH 5.5)], 5 µL FMN (25 µM for WT protein), or water (FMN-binding mutants), 5 µL GUS, and 30 µL 4-MUG (varying concentration). Reactions were initiated by addition of substrate, and reactions were continuously monitored with excitation at 350 nm and emission at 450 nm in a BMG labtech PHER-Astar plate reader. Initial velocities from the resultant data were fit by linear regression with a custom MATLAB program, and k_{cat}, K_M, and k_{cat}/K_M were determined in SigmaPlot 13.0.

Accession numbers

Coordinates and structure factors have been deposited in the Protein Data Bank with accession numbers 6MVF, 6MVG, and 6MVH for *Fp2*GUS, *Rg3*GUS, and *Rh2*GUS, respectively.

Appendix A. Supplementary Data

Supplementary data to this article can be found online at https://doi.org/10.1016/j.jmb.2019.01.013.

References

[1] J. Qin, R. Li, J. Raes, M. Arumugam, K.S. Burgdorf, C. Manichanh, T. Nielsen, N. Pons, F. Levenez, T. Yamada, D.R. Mende, J. Li, J. Xu, S. Li, D. Li, J. Cao, B. Wang, H. Liang, H. Zheng, Y. Xie, J. Tap, P. Lepage, M. Bertalan, J.M. Batto, T. Hansen, D. Le Paslier, A. Linneberg, H.B. Nielsen, E. Pelletier, P. Renault, T. Sicheritz-Ponten, K. Turner, H. Zhu, C. Yu, S. Li, M. Jian, Y. Zhou, Y. Li, X. Zhang, S. Li, N. Qin, H. Yang, J. Wang, S. Brunak, J. Doré, F. Guarner, K. Kristiansen, O. Pedersen, J. Parkhill, J. Weissenbach, P. Bork, S.D. Ehrlich, J. Wang, M. Antolin, F. Artiguenave, H. Blottiere, N. Borruel, T. Bruls, F. Casellas, C. Chervaux, A. Cultrone, C. Delorme, G. Denariaz, R. Dervyn, M. Forte, C. Friss, M. Van De Guchte, E. Guedon, F. Haimet, A. Jamet, C. Juste, G. Kaci, M. Kleerebezem, J. Knol, M. Kristensen, S. Layec, K. Le Roux, M. Leclerc, E. Maguin, R. Melo Minardi, R. Oozeer, M. Rescigno, N. Sanchez, S. Tims, T. Torrejon, E. Varela, W. De Vos, Y. Winogradsky, E. Zoetendal, A human gut microbial gene catalogue established by metage-nomic sequencing, Nature (2010) https://doi.org/10.1038/nature08821.

[2] V. Lombard, H. Golaconda Ramulu, E. Drula, P.M. Coutinho, B. Henrissat, The carbohydrate-active enzymes database (CAZy) in 2013, Nucleic Acids Res. (2014) https://doi.org/10.1093/nar/gkt1178.

[3] G. den Besten, K. van Eunen, A.K. Groen, K. Venema, D.-J. Reijngoud, B.M. Bakker, The role of short-chain fatty acids in the interplay between diet, gut microbiota, and host energy metabolism, J. Lipid Res. (2013) https://doi.org/10.1194/jlr.R036012.

[4] R.M. Pollet, E.H. D'Agostino, W.G. Walton, Y. Xu, M.S. Little, K.A. Biernat, S.J. Pellock, L.M. Patterson, B.C. Creekmore, H.N. Isenberg, R.R. Bahethi, A.P. Bhatt, J. Liu, R.Z. Gharaibeh, M.R. Redinbo, An atlas of β-glucuronidases in the human intestinal microbiome, Structure 25 (2017) 967-977.e5.

[5] S.J. Pellock, W.G. Walton, K.A. Biernat, D. Torres-Rivera, B.C. Creekmore, Y. Xu, J. Liu, A. Tripathy, L.J. Stewart, M.R. Redinbo, Three structurally and functionally distinct β-

glucuronidases from the human gut microbe *Bacteroides uniformis*, J. Biol. Chem. (2018) https://doi.org/10.1074/jbc.RA118.005414.

[6] K.S. Saitta, C. Zhang, K.K. Lee, K. Fujimoto, M.R. Redinbo, U.A. Boelsterli, Bacterial β-glucuronidase inhibition protects mice against enteropathy induced by indomethacin, ketoprofen or diclofenac: mode of action and pharmacokinetics, Xenobiotica (2014) https://doi.org/10.3109/00498254.2013.811314.

[7] U.A. Boelsterli, M.R. Redinbo, K.S. Saitta, Multiple NSAID-induced hits injure the small intestine: underlying mechanisms and novel strategies, Toxicol. Sci. 131 (2013) 654–667.

[8] G.J. Dutton, Glucuronic acid, free and combined, biochemistry, pharmacology, and medicine, Academic Press, New York, 1966.

[9] N.T. Porter, E.C. Martens, The critical roles of polysaccharides in gut microbial ecology and physiology, Annu. Rev. Microbiol. (2017) https://doi.org/10.1146/annurev-micro-102215-095316.

[10] B.D. Wallace, H. Wang, K.T. Lane, J.E. Scott, J. Orans, J.S. Koo, M. Venkatesh, C. Jobin, L.-A. Yeh, S. Mani, M.R. Redinbo, Alleviating Cancer drug toxicity by inhibiting a bacterial enzyme, Science (80) 330 (2010) 831–835.

[11] A.B. Roberts, B.D. Wallace, M.K. Venkatesh, S. Mani, M.R. Redinbo, Molecular insights into microbial β-glucuronidase inhibition to abrogate CPT-11 toxicity, Mol. Pharmacol. 84 (2013) 208–217.

[12] B.D. Wallace, A.B. Roberts, R.M. Pollet, J.D. Ingle, K.A. Biernat, S.J. Pellock, M.K. Venkatesh, L. Guthrie, S.K. O'Neal, S.J. Robinson, M. Dollinger, E. Figueroa, S.R. McShane, R.D. Cohen, J. Jin, S.V. Frye, W.C. Zamboni, C. Pepe-Ranney, S. Mani, L. Kelly, M.R. Redinbo, Structure and inhibition of microbiome β-glucuronidases essential to the alleviation of cancer drug toxicity, Chem. Biol. 22 (2015) 1238–1249.

[13] S.F. Altschul, W. Gish, W. Miller, E.W. Myers, D.J. Lipman, Basic local alignment search tool, J. Mol. Biol. (1990) https://doi.org/10.1016/S0022-2836(05)80360-2.

[14] T.N. Petersen, S. Brunak, G. von Heijne, H. Nielsen, SignalP 4.0: discriminating signal peptides from transmembrane regions, Nat. Methods (2011) https://doi.org/10.1038/nmeth.1701.

[15] J.A. Gerlt, J.T. Bouvier, D.B. Davidson, H.J. Imker, B. Sadkhin, D.R. Slater, K.L. Whalen, Enzyme function initiative-enzyme similarity tool (EFI-EST): A web tool for generating protein sequence similarity networks, Biochim. Biophys. Acta Protein Proteomics (2015) https://doi.org/10.1016/j.bbapap.2015.04.015.

[16] J. Schmid, N. Sperl, V. Sieber, A comparison of genes involved in sphingan biosynthesis brought up to date, Appl. Microbiol. Biotechnol. (2014) https://doi.org/10.1007/s00253-014-5940-z.

[17] P.L. Pham, I. Dupont, D. Roy, G. Lapointe, J. Cerning, Production of exopolysaccharide by *Lactobacillus rhamnosus* R and analysis of its enzymatic degradation during prolonged fermentation, Appl. Environ. Microbiol. (2000) https://doi.org/10.1128/AEM.66.6.2302-2310.2000.

[18] W. Hashimoto, K. Murata, α-ʟ-Rhamnosidase of *Sphingomonas* sp. R1 producing an unusual exopolysaccharide of Sphingan, Biosci. Biotechnol. Biochem. (1998) https://doi.org/10.1271/bbb.62.1068.